Detection of liquid–vapor–solid triple contact line in two-phase heat transfer phenomena using high-speed infrared thermometry

Citation: Kim, Hyungdae, and Jacopo Buongiorno. "Detection of Liquid–vapor–solid Triple Contact Line in Two-Phase Heat Transfer Phenomena Using High-Speed Infrared Thermometry." International Journal of Multiphase Flow 37, no. 2 (March 2011): 166–172.

As Published: http://dx.doi.org/10.1016/j.ijmultiphaseflow.2010.09.010

Publisher: Elsevier

Persistent URL: http://hdl.handle.net/1721.1/105170

Version: Author's final manuscript: final author's manuscript post peer review, without publisher's formatting or copy editing

Detection of Liquid-Vapor-Solid Triple Contact Line in Two-Phase Heat Transfer Phenomena Using High-Speed Infra-Red Thermometry

Hyungdae Kim[a,b], Jacopo Buongiorno[a *]

[a] Nuclear Science and Engineering Department, Massachusetts Institute of Technology, Cambridge, MA 02139, USA

[b] Nuclear Engineering Department, Kyung Hee University, Youngin, Republic of Korea

* Corresponding author: jacopo@mit.edu, +1-617-253-7316

Abstract

Heat transfer in complex physical situations such as nucleate boiling, quenching and dropwise condensation is strongly affected by the presence of a liquid-vapor-solid triple contact line, where intense energy transfer and phase change occur. A novel experimental technique for the detection of the liquid-vapor-solid line in these situations is presented. The technique is based on high-speed infrared (IR) thermometry through an IR-transparent silicon wafer heater; hence the name DEPIcT, or DEtection of Phase by Infrared Thermometry. Where the heater surface is wet, the IR camera measures the temperature of the hot water in contact with the heater. On the other hand, where vapor (whose IR absorptivity is very low) is in contact with the heater, the IR light comes from the cooler water beyond the vapor. The resulting IR image appears dark (cold) in dry spots and bright (hot) in wetted area. Using the contrast

between the dark and bright areas, we can visualize the distribution of the liquid and gas phases in contact with the heater surface, and thus identify the liquid-vapor-solid contact line. In other words, we measure temperature *beyond* the surface to detect phases *on* the surface. It was shown that even small temperature differences (~1°C) can yield a sharp identification of the contact line, within about 100 μm resolution. DEPIcT was also shown to be able to detect thin liquid layers, through the analysis of interference patterns.

Keywords: liquid thin film; microlayer; boiling; DEPIcT

1. Introduction

Complex two-phase heat transfer phenomena such as nucleate boiling, critical heat flux, quenching and dropwise condensation are characterized by the presence of a liquid-vapor-solid contact line on the surface from/to which the heat is transferred. For example, in nucleate boiling, a significant fraction (but not all [Kim 2009]) of the energy needed for bubble growth may come from evaporation of a liquid meniscus, or microlayer, underneath the bubble itself, as shown in Fig. 1a. As the liquid-vapor-solid line at the edge of the meniscus retreats, a circular dry patch in the middle of the bubble is exposed; the speed of the triple line retreat is one measure of the ability of the microlayer to transfer heat to the bubble. At very high heat fluxes, near the upper limit of the nucleate boiling regime, also known as Critical Heat Flux (CHF), the situation is characterized by larger dry areas on the surface, dispersed within an interconnected network of liquid menisci (see Fig. 1b) [Chung and No 2003].

In quenching heat transfer, which refers to the rapid cooling of a very hot object by immersion in a cooler liquid, the process is initially dominated by film boiling. In film boiling a continuous vapor film completely separates the liquid phase from the solid surface; however, as the temperature gets closer to the Leidenfrost point, intermittent and short-lived liquid-solid contacts occur at discrete locations on the surface, thus creating liquid-vapor-solid interfaces

once again (see Fig. 1c). Ultimately, if bubble nucleation ensues at such contact points, the vapor film is disrupted and the heat transfer regime transitions from film boiling to transition boiling.

Finally, in dropwise condensation, the phase transition from vapor to liquid occurs via formation of discrete droplets on the surface (see Fig. 1d) [Rose 2002], and the resulting liquid-vapor-solid triple line is where heat transfer is most intense.

To gain insight into and enable mechanistic modeling of all these two-phase heat transfer phenomena, there is clearly a need to detect the liquid-vapor-solid triple contact line and measure its physical characteristics (extension, speed, temperature).

Two-phase flow and heat transfer diagnostics is a rich field, which has produced several tools for probing certain aspects of the afore-mentioned phenomena. We will focus here on instruments that detect phases. For the purpose of this study, phase detectors can be divided into two broad categories: 'bulk phase detectors' and 'surface phase detectors'. The bulk phase detectors detect phases within the bulk of the flow, away from the solid surface; they include conductivity and optical probes [Kim et al. 2000, Barrau et al. 1999] and wire-mesh probes [Prasser et al. 1998]. They are intrusive instruments and generally have low (discrete)

spatial resolution. On the other hand, X-ray and γ-ray tomography is non-intrusive, but rather costly/cumbersome as the radiation source has to be rotated at high speed around the test section, which also may limit the time and/or space resolution of the technique; ultra-fast approaches have been developed to increase the time and space resolution in recent years [Hori et al. 2000, Bieberle et al. 2009]. More suitable for detection of the triple contact line are the surface phase detectors. These include high-speed video, whose usefulness typically is limited by poor optical access to the surface due to the interference from rising bubbles, and total reflection, which is rather simple and effective, but requires a heater that is completely transparent to visible light, e.g., an indium-tin-oxide film on sapphire or borosilicate glass substrate [Nishio and Tanaka 2004].

In this paper we describe a different (novel) technique, based on infrared (IR) thermometry *through* an infrared-transparent solid surface, which exploits temperature (and absorptivity) differences to detect the liquid-vapor-solid triple contact line. We call this technique DEPIcT, or DEtection of Phase by Infrared Thermometry. DEPIcT is first described in Section 2; the spatial uncertainties and sensitivities in the identification of the triple contact line are discussed in Section 3; the ability of DEPIcT to detect thin films is discussed in Section 4.

2. Infrared thermometry to detect liquid-gas-solid contact line

An IR camera is used to detect the phases present on a heated surface. The key feature of this technique is to use a heater material that is IR transparent (e.g. optical grade silicon wafer), and a fluid that has a very high IR absorptivity (e.g. water). The IR camera is placed below the heater, while the fluid lies on top (Fig. 2). Where the heater surface is wet, the IR camera measures the temperature of the hot water in contact with the heater. On the other hand, where vapor (whose IR absorptivity is very low) is in contact with the heater, the IR light comes from the cooler water beyond the vapor. The resulting IR image appears dark (cold) in dry spots and bright (hot) in wetted area. Using the contrast between the dark and bright areas, we can visualize the distribution of the liquid and gas phases in contact with the heater surface, and thus identify the liquid-vapor-solid contact line. In other words, we measure temperature *beyond* the surface to detect phases *on* the surface. This approach distinguishes DEPIcT from the now-established IR thermometry technique with IR-opaque heaters [Theofanous et al. 2002, Wagner and Stephan 2009, Gerardi et al. 2010], where the temperature measured is the temperature of the surface, which makes it hard to identify phases on the surface conclusively.

The IR camera used in this study is a SC6000, FLIR Systems Inc., with an IR wavelength range of 3-5 μm. Optical grade silicon wafer with the following properties was used as the heater: <100> orientation, P/Boron-doped, electrical resistivity 5-25 Ω-cm, thickness 380±25 μm, and double side polished. The relatively high electrical conductivity of this doped silicon made it possible to use direct (Joule) heating in boiling experiments. The silicon wafer heater is completely opaque to visible light, but transparent to IR.

A simple experiment with a sliding droplet was conducted first, to verify the optical properties of the wafer and demonstrate the technique (Fig. 3). The liquid was pre-heated to ~30°C, while the wafer and background were at room temperature (~24°C); as a result, in the IR video the sliding droplet appears brighter than the background, and thus easily distinguishable. Comparison of high-speed video (HSV) taken from above the wafer with IR video taken *through* the wafer clearly shows that the DEPIcT technique precisely and sharply captures the dynamics of liquid flow on the surface of the wafer, including the triple contact line.

In our lab the HSV is acquired with a Phantom v7.1 camera by Vision Research, Inc., capable of up to 4800 fps at full 800×600 pixel resolution.

3. Uncertainties and Sensitivities

Since DEPIcT uses a temperature measurement to detect the triple contact line, it is important to quantify the uncertainties and sensitivities involved in the IR temperature measurement per se and the subsequent identification of the triple contact line from the IR image. First, the IR camera used in this study has a temperature resolution of 0.025°C, a maximum frame rate of 125 fps at full spatial resolution of 640×512 pixels and higher frame rates at a subset of the total image, i.e. 1000 fps at 144×144 pixels. The actual spatial resolution depends obviously on the physical size of the object being imaged. For example, if we are interested in imaging an area of 1 cm^2 and use 100×100 pixels, the spatial resolution is 100 μm. To quantify the uncertainties and sensitivities of the triple-contact-line detection, a series of tests with static droplets was conducted at various temperatures. The experimental setup for these tests is shown in Fig. 4. The background water was kept at room temperature (24.3°C), while the temperature of the wafer and the droplet hanging under it were varied from 25.6 to 30°C. Figure 5 shows the measured IR intensity (counts) of the dry and wet regions of the wafer surface for different temperatures of the droplet-wafer system. It can be seen that, although the wafer and droplet are at the same temperature, their signals are very different; this is due to the differences in the temperature of the droplet hanging under the wafer and the background water, and makes it possible to distinguish dry surface from wet surface quite clearly. Figure

6 shows the IR intensity profile near the edge of droplets at various temperatures. If we assume the inflection point in the curves to be the nominal location of the triple contact line, the range over which the IR intensity changes significantly (~50%) is about 100 μm. Therefore, the triple contact line on the surface can be identified within 100 μm. Finally, note that the IR intensity change across the contact line is rather sharp even when the temperature difference between the wafer-droplet system and the background becomes as low as 1.3°C (=25.6-24.3).

As an additional check of the ability of the technique to capture the contact line, we conducted a test with static air bubbles attached to the top surface of the wafer. This test was isothermal, i.e. the wafer, air and water were all at the same (room) temperature. Figure 7a shows the overall IR image of the surface, where the bubbles are clearly visible. Figure 7b shows the IR intensity profile near the edge of a bubble; the triple contact line is easily identifiable also in this situation. In Figure 7, the difference in the IR signal is due to the depth-of-field (DOF) effect of the IR optical configuration used. DOF is the distance along the optical axis on either side of the focus point that remains within acceptable focus. The liquid in contact with the silicon wafer is “in focus” while the background liquid is “out of focus”. The resulting IR

intensity is higher for the liquid in contact with the wafer (wet region) than for the liquid beyond the air (dry region), even though temperature and emissivity are the same for both liquids in this test. In summary, if a temperature gradient exists, it is the dominant contrast mechanism; however, Figure 7 shows that the DOF effect is also capable of creating contrast at the triple contact line.

4. Detection of thin films

A key question for the new technique concerns its ability to distinguish a surface that is truly dry from one covered by a thin liquid film. As discussed in the Introduction, in boiling heat transfer the area underneath a growing bubble is covered by a thin (and rapidly evaporating) liquid film, which can be only a few microns thick [Cooper and Lloyd 1969]. At high heat flux, near CHF, there is a network of thin liquid films sloshing on the surface [Nishio and Tanaka 2004, Chung and No 2003]. For data interpretation and development of boiling heat transfer models, it is important to determine the location (and possibly the thickness) of these films.

Our IR camera has a wavelength detection range of 3-5 μm; in this range the penetration length

of light in water varies from a minimum of 1 μm (at 3.0 μm) to a maximum of 100 μm (at 3.8 μm) [Wieliczka et al. 1989]; therefore, at first, one might conclude that the minimum liquid film thickness that can give full liquid-vapor contrast with our camera is 100 μm. In fact, even thinner liquid films can be detected through the analysis of interference fringe patterns created by the passage of IR light through the films. To illustrate this concept, we conducted a series of tests with wedge-type planar films, as shown in Figure 8. The thin films were created by two flat silicon sheets (60 mm × 20 mm) separated by sheets of clear plastic tape with a thickness of 50 μm; by varying the number of the sheets, we controlled the slope of the films. The IR image for one particular configuration is shown in Figure 9a. The IR intensity profile is shown in Figure 9b. Interference fringe patterns are clearly visible. The fringe spacing, Δ, is related to the IR wavelength and slope of the film by the following relation [Dumin 1967]:

$$\Delta = \frac{\lambda}{2n}\frac{L}{t} \qquad (1)$$

where λ is the IR wavelength, n is the index of refraction of the film layer, t/L is the slope of the film where t and L are the thickness of the plastic sheets and length of the base substrate, respectively. Equation 1 was verified by varying the slope of the film in the tests and calculating the corresponding IR wavelength from Eq. 1. The results are shown in Figure 9;

the wavelength is approximately constant and well within the IR range of our camera, as expected.

Next, we used a lens, to create an axi-symmetric curved film off a silicon plate (see Figure 8b), as that is the geometry of the microlayer underneath a growing bubble. Figure 10 shows the interference rings both in the presence and absence of water between the lens and the silicon plate. The lens radius of curvature inferred from the ring spacing ranges from 256 to 282 mm, which is in good agreement with the actual radius of curvature (257 mm) provided by the lens manufacturer.

Lastly, we decided to demonstrate the technique for an individual vapor bubble, nucleating and growing off the surface of the silicon wafer. This case is interesting because it combines the elements analyzed separately in the previous sections, i.e. temperature gradients and thin films, but in a dynamic situation. Boiling was induced by resistively heating the silicon wafer with a DC power supply via Au/Cr metal pads for electrical connection. The IR images were taken from below the wafer, while boiling occurred on the top face of the wafer (as shown in Fig. 2). Figure 11a shows the temporally and spatially synchronized images of the HSV and IR

cameras for the bubble. The IR images show various features of the growing bubble, including a dry (dark) spot at the center of the bubble, a wet (bright) region away from the bubble, and, up to 5 ms, an intermediate (gray) region. The presence of interference rings in this intermediate region (see Figure 11b) suggests the presence of a liquid film at the base of the bubble. This is the so-called microlayer; note that detection of the microlayer via analysis of interference patterns is not a new approach, though in the past was done predominantly with visible light [Judd and Hwang 1976, Fath and Judd 1978, Koffman and Plessett 1983]. Koffman and Plesset [1983] developed a technique to accurately measure the microlayer thickness profiles beneath small, short-lived bubbles using laser interferometry combined with high speed cinematography. However, the interferometry technique of Koffman and Plesset had more limited capabilities than DEPIcT because it could not measure the phase distribution on the surface, but only the thickness of the microlayer.

From the spacing between rings, it was possible to reconstruct the shape (slope) of the microlayer vs time, as shown in Figure 12. After the microlayer has evaporated (>5 ms) the triple contact line starts to advance toward the bubble axis, as the bubble is detaching from the surface under the effect of buoyancy (Fig. 11, frames 6 ms and higher). The image at 14 ms

shows that only the tiny tail of the bubble is attached to the heater surface.

5. Conclusion

DEPIcT, a new high-speed phase detection technique suitable for two-phase heat transfer studies, was presented. It is based on IR thermometry through an IR-transparent heater. DEPIcT was shown to be able to detect the liquid-vapor-solid triple line accurately in simple situations such as sliding and static droplets and static bubbles. DEPIcT can also be used to detect thin liquid films on the surface through the analysis of interference patterns. This aspect was demonstrated for the microlayer under a growing bubble in nucleate boiling.

Acknowledgements

This work has been made possible by a Seed Fund grant from the MIT Energy Initiative, and was partially supported by the Korea Science and Engineering Foundation (KOSEF) grant funded by the Korea government (MEST) (No. 2010-0018761). Prof. Karl Berggren and Dr. Sebastian Strobel of MIT are acknowledged for providing the silicon wafers used in this study. Thanks to Dr. Truc-Nam Dinh of the Idaho National Laboratory (INL) for providing useful comments on the work.

References

- E. Barrau, N. Rivière, Ch. Poupot and A. Cartellier, 1999, “Single and double optical probes in air-water two-phase flows: real time signal processing and sensor performance”, Int. J. Multiphase Flow, 25(2), 229-256.
- M. Bieberle, F. Fischer, E. Schleicher, D. Koch, H.-J. Menz, H.-G. Mayer, U. Hampel, 2009, “Experimental two-phase flow measurement using ultra fast limited-angle-type electron beam X-ray computed tomography”, Experiments in Fluids, v 47, n 3, p 369-378.
- H. J. Chung, H. C. No, 2003, Simultaneous visualization of dry spots and bubbles for pool boiling of R-113 on a horizontal heater, International Journal of Heat and Mass Transfer 46 2239–2251.
- M. G. Cooper, A. J. P. Lloyd, 1969, “The Microlayer in Nucleate Pool Boiling”, Int. J. Heat Mass Transfer, 12, pp. 895-913.
- D. J. Dumin, 1967, “Measurement of Film Thickness Using Infrared Interference,” Rev. Sci. Instrum., 38(8), pp. 1107-1109.
- H. S. Fath and R. L. Judd, 1978, "Influence of system pressure on microlayer evaporation heat transfer", J. of Heat Transfer, Vol. 100, pp. 49-55.
- C. Gerardi, J. Buongiorno, L. W. Hu, T. McKrell, 2010, “Study of Bubble Growth in Water Pool Boiling Through Synchronized, Infrared Thermometry and High-Speed Video”, Int. J. Heat Mass Transfer, 53, 4185–4192.
- K. Hori, T. Fujimoto, K. Kawamishi, H. Nishikawa, 2000, “Development of an ultrafast X-ray computed tomography scanner system: application for measurement of instantaneous void distribution of gas-liquid two-phase flow”, Heat Transfer-Asian Research, v 29, n 3, p 155-65.
- R. L. Judd and K. S. Hwang, 1976, "A comprehensive model for nucleate pool boiling heat tr

ansfer including microlayer evaporation", J. of Heat Transfer, pp. 623-629.

- S. Kim, X.Y. Fu, X. Wang and M. Ishii, 2000, “Development of the miniaturized four-sensor conductivity probe and the signal processing scheme”, Int. J. Heat Mass Transfer, 43(22), 4101-4118.
- J. Kim, 2009, “Review of Nucleate Pool Boiling Heat Transfer Mechanisms”, Int. J. Multiphase Flow, 35, 1067-1076.
- L. D. Koffman and M. S. Plessett, 1983, "Experimental observations of the microlayer in vapor bubble growth on a heated solid", J. Heat Transfer, Vol. 105, pp. 625-632.
- S. Nishio and H. Tanaka, 2004, “Visualization of boiling structures in high-heat flux pool-boiling”, Int. J. Heat Mass Transfer, 47, 4559-4568.
- H.M. Prasser, A. Bottger, J. Zschau, 1998, “A new electrode-mesh tomography for gas–liquid flows,” Flow Measurement and Instrumentation, 9, 111–119.
- J. W. Rose, 2002, “Dropwise condensation theory and experiment: a review,” Proceedings of the Institution of Mechanical Engineers, Part A: Journal of Power and Energy, vol. 216 (2), pp. 115-128.
- G. Strotos, M. Gavaises, A. Theodorakakos, G. Bergeles, 2008, Numerical investigation on the evaporation of droplets depositing on heated surfaces at low Weber numbers, International Journal of Heat and Mass Transfer 49 (7-8) 1516-1529.
- T. G. Theofanous, J. P. Tu, A. T. Dinh and T. N. Dinh, 2002, The Boiling Crisis Phenomenon, J. Experimental Thermal Fluid Science, P.I: pp. 775-792, P.II: pp. 793-810, 26 (6-7).
- T. G. Theofanous, T. N. Dinh, 2006, High heat flux boiling and burnout as microphysical phenomena: mounting evidence and opportunities, Multiphase Science and Technology 18 (3) 251-276.

- E. Wagner and P. Stephan, 2009, High-resolution measurements at nucleate boiling of pure FC-84 and FC-3284 and its binary mixtures, Journal of Heat Transfer, v. 131, n. 12, p. 121008.
- D. M. Wieliczka, S. Weng, M. R. Querry, 1989, Wedge shaped cell for highly absorbent liquids: infrared optical constants of water, Applied Optics 28 (9) 1714 -1719.
- L. Zhang, M. Shoji, 2003, Nucleation site interaction in pool boiling on the artificial surface, International Journal of Heat and Mass Transfer 46 (3) 513-522.

FIGURE CAPTIONS

Figure 1. Representation of physical situation for (a) bubble growth, (b) high-heat-flux nucleate boiling, (c) Leidenfrost point, and (d) dropwise condensation.

Figure 2. Schematic diagram of the DEPIcT technique. The IR camera takes an image through the wafer.

Figure 3. Droplet sliding on a vertical silicon wafer. Comparison of the HSV (left) and IR (right) images taken from the front and back of the wafer, respectively. The sharpness of the IR image through the wafer confirms that the wafer is transparent to IR.

Figure 4. Experimental set-up for static droplet tests.

Figure 5. IR intensity emitted by the droplet and wafer at various temperatures.

Figure 6. 1D IR intensity profile at the droplet contact line for various droplet-wafer temperatures (T_{room}=24.3^{o}C for all cases).

Figure 7. (a) IR image of static air bubbles on top of the wafer under isothermal conditions at 24.1^{o}C, and (b) 1D IR intensity profile near the edge of a bubble.

Figure 8. Experimental setup for detection of (a) planar and (b) curved thin films via interference fringe patterns.

Figure 9. (a) IR image (b) and IR intensity profile for a planar film of slope 0.0037. (c) IR

wavelength calculated from Eq. 1 for films of various slopes.

Figure 10. (a) IR interference rings from an axi-symmetric curved film with a radius of curvature of 257 mm. (b) Same as (a) but with no water between the lens and the silicon plate.

Figure 11. Bubble nucleation, growth and departure in saturated water on an electrically-heated silicon wafer: (a) synchronized HSV and IR pictures. (b) interference rings are clearly visible between the dry center of the bubble base and the outer wet region of the wafer.

Figure 12. Microlayer shape vs time underneath a growing bubble.

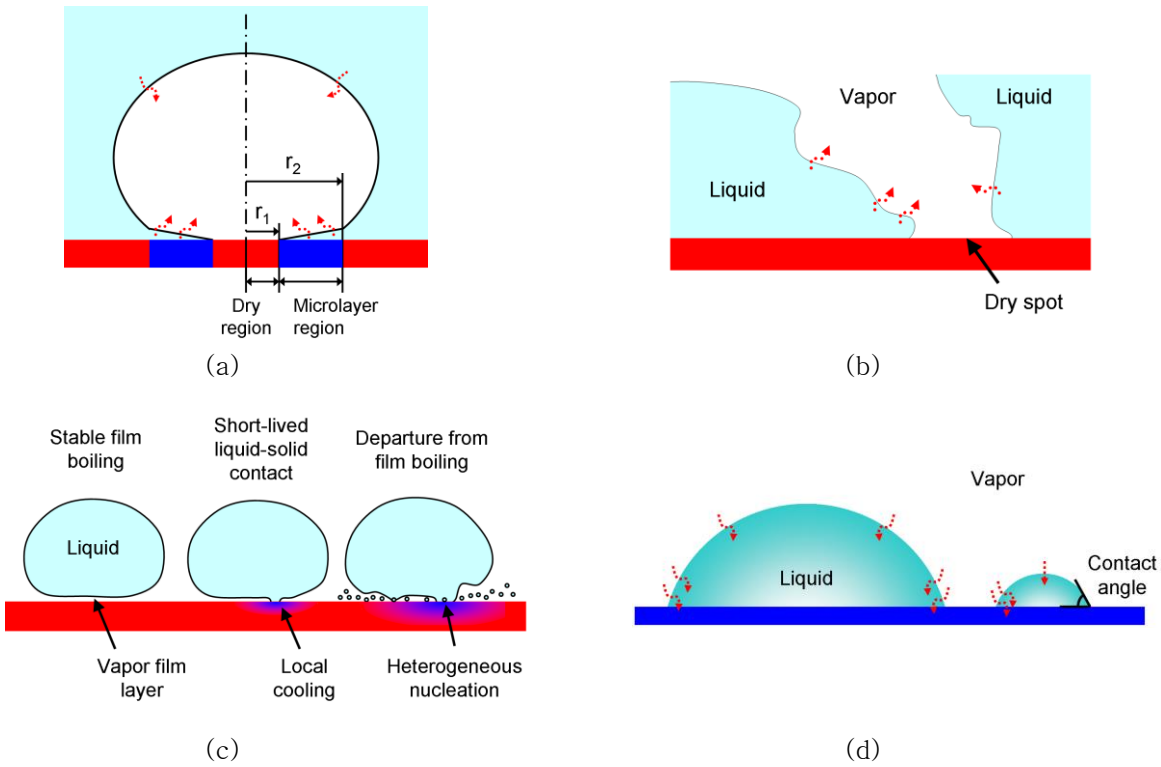

Figure 1. Representation of physical situation for (a) bubble growth, (b) high-heat-flux nucleate boiling, (c) Leidenfrost point, and (d) dropwise condensation.

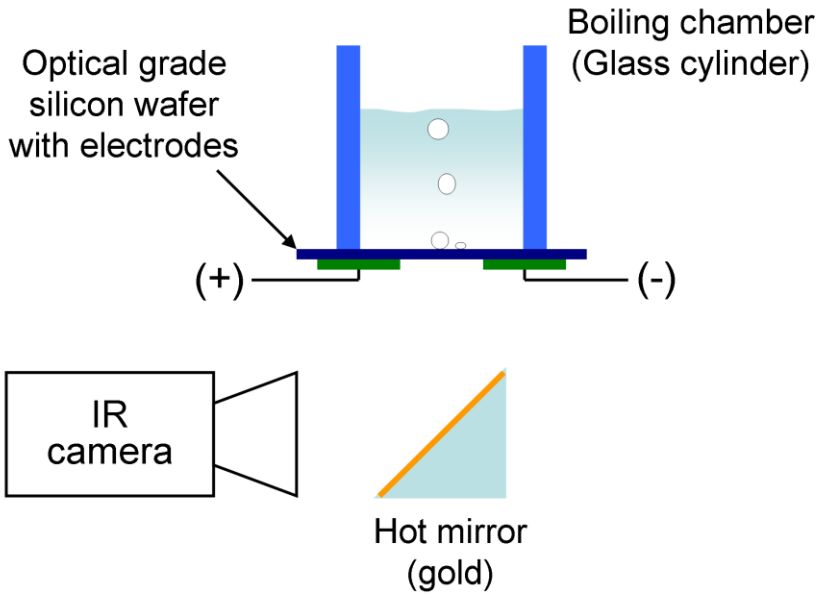

Figure 2. Schematic diagram of the DEPIcT technique. The IR camera takes an image through the wafer.

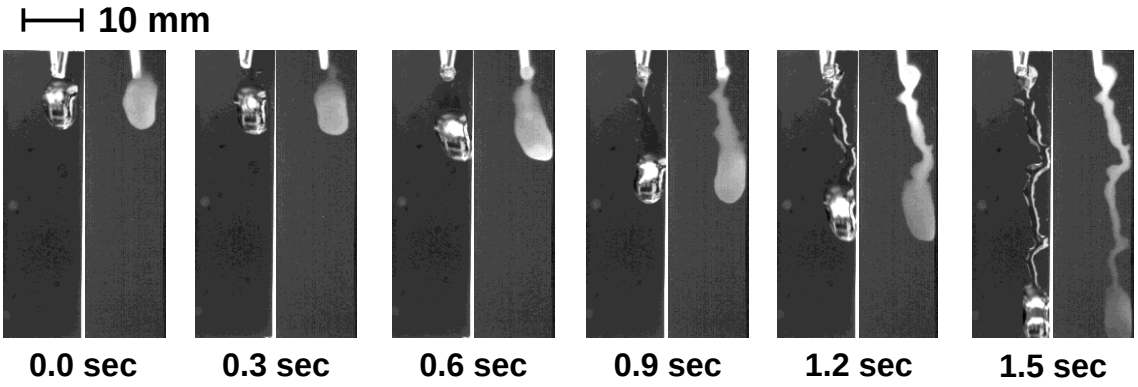

Figure 3. Droplet sliding on a vertical silicon wafer. Comparison of the HSV (left) and IR (right) images taken from the front and back of the wafer, respectively. The sharpness of the IR image through the wafer confirms that the wafer is transparent to IR.

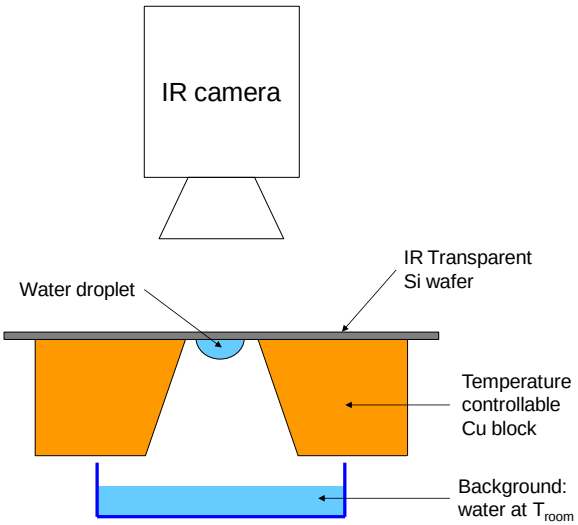

Figure 4. Experimental set-up for static droplet tests.

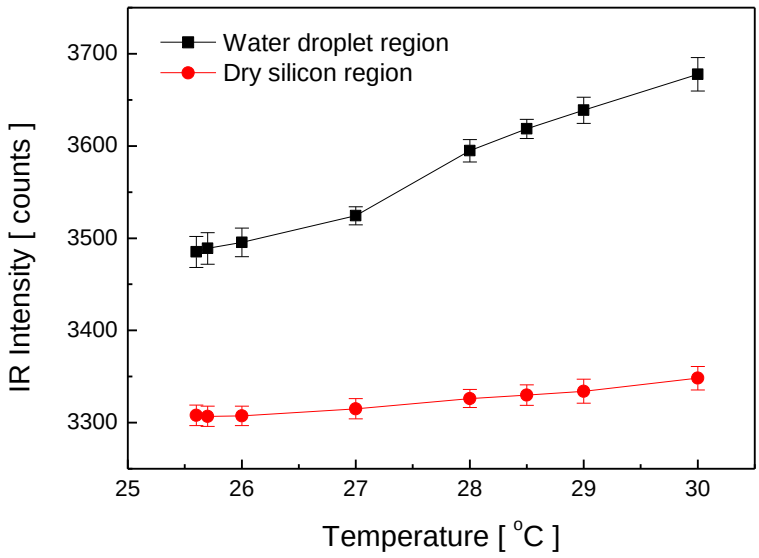

Figure 5. IR intensity emitted by the droplet and wafer at various temperatures.

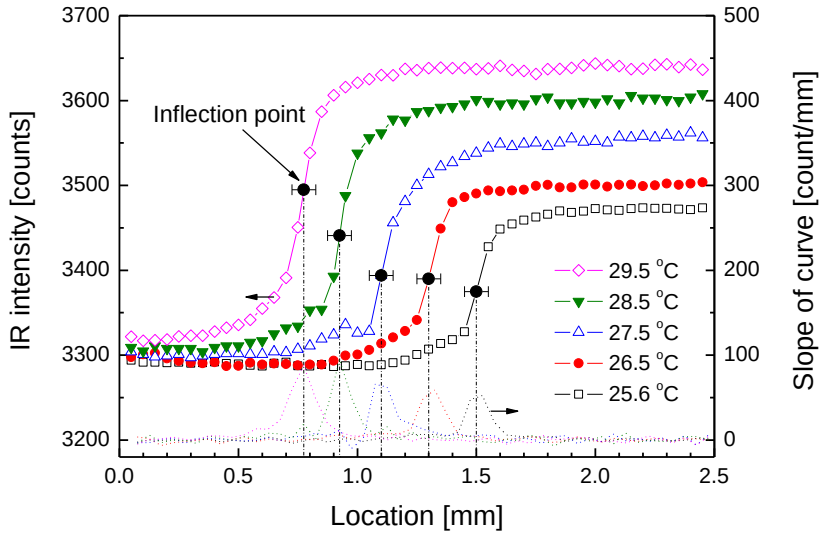

Figure 6. 1D IR intensity profile at the droplet contact line for various droplet-wafer temperatures (T_{room}=24.3^{o}C for all cases).

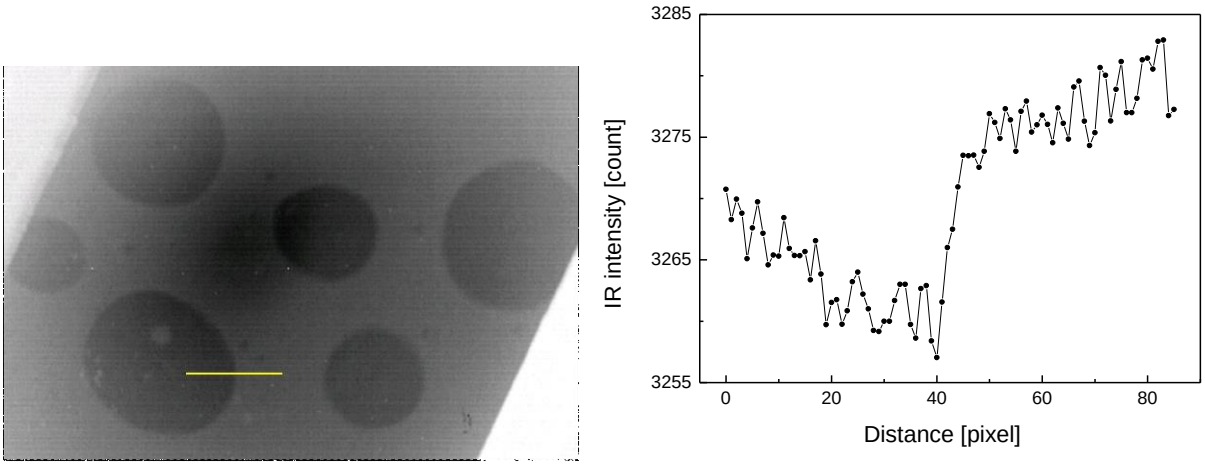

(a) (b)

Figure 7. (a) IR image of static air bubbles on top of the wafer under isothermal conditions at 24.1^{o}C, and (b) 1D IR intensity profile near the edge of a bubble.

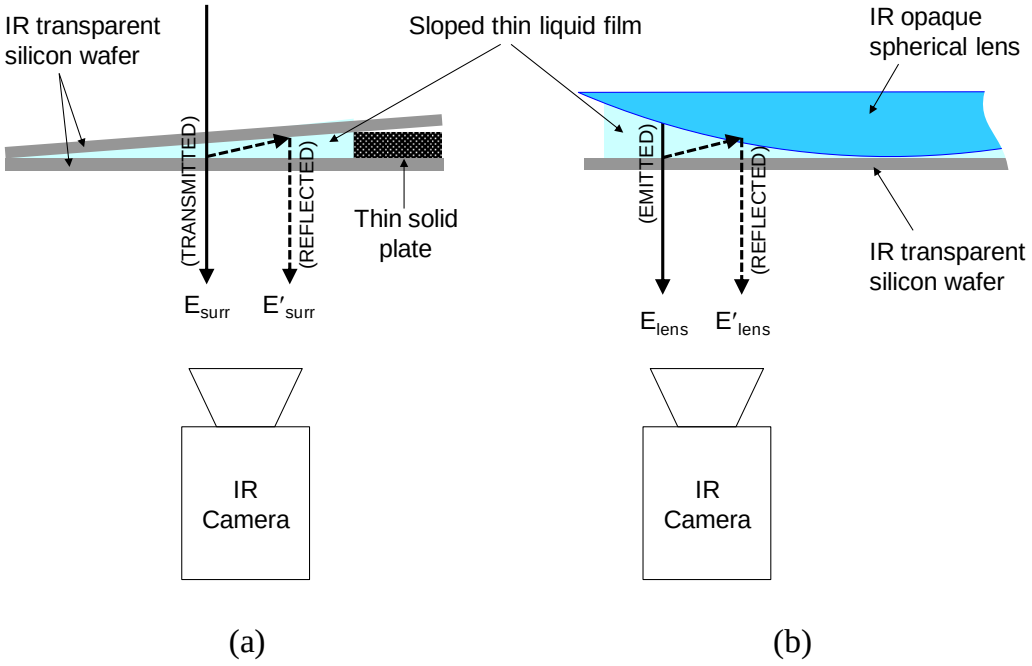

Figure 8. Experimental setup for detection of (a) planar and (b) curved thin films via interference fringe patterns.

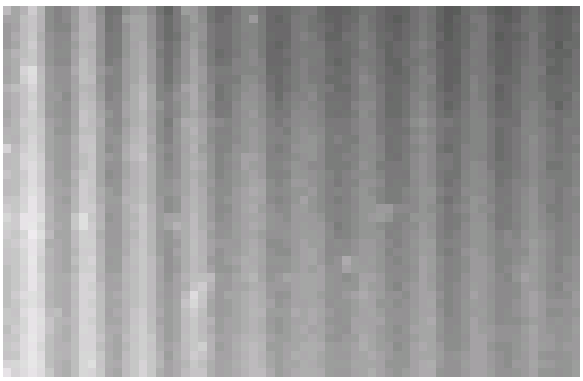

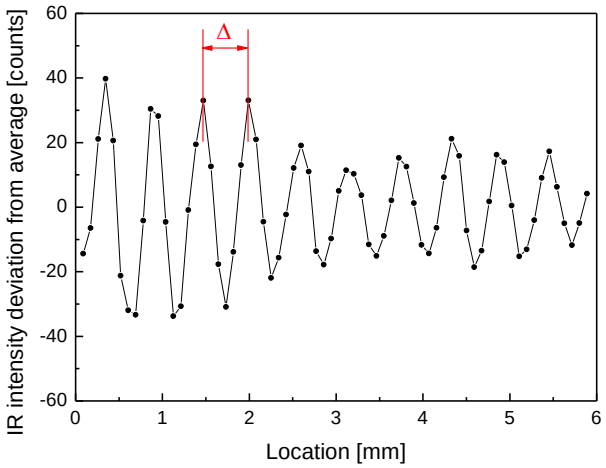

(a) (b)

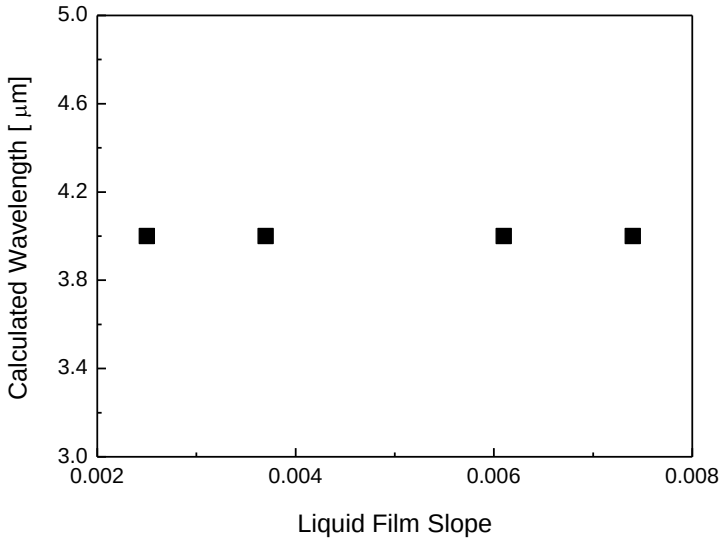

(c)

Figure 9. (a) IR image (b) and IR intensity profile for a planar film of slope 0.0037. (c) IR wavelength calculated from Eq. 1 for films of various slopes.

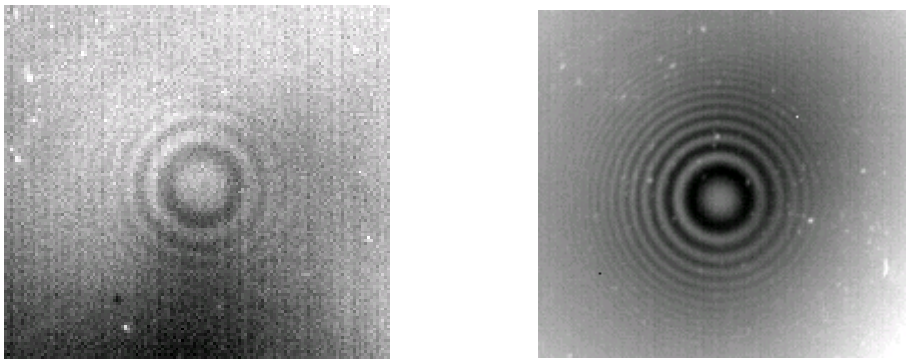

(a) (b)

Figure 10. (a) IR interference rings from an axi-symmetric curved film with a radius of curvature of 257 mm. (b) Same as (a) but with no water between the lens and the silicon plate.

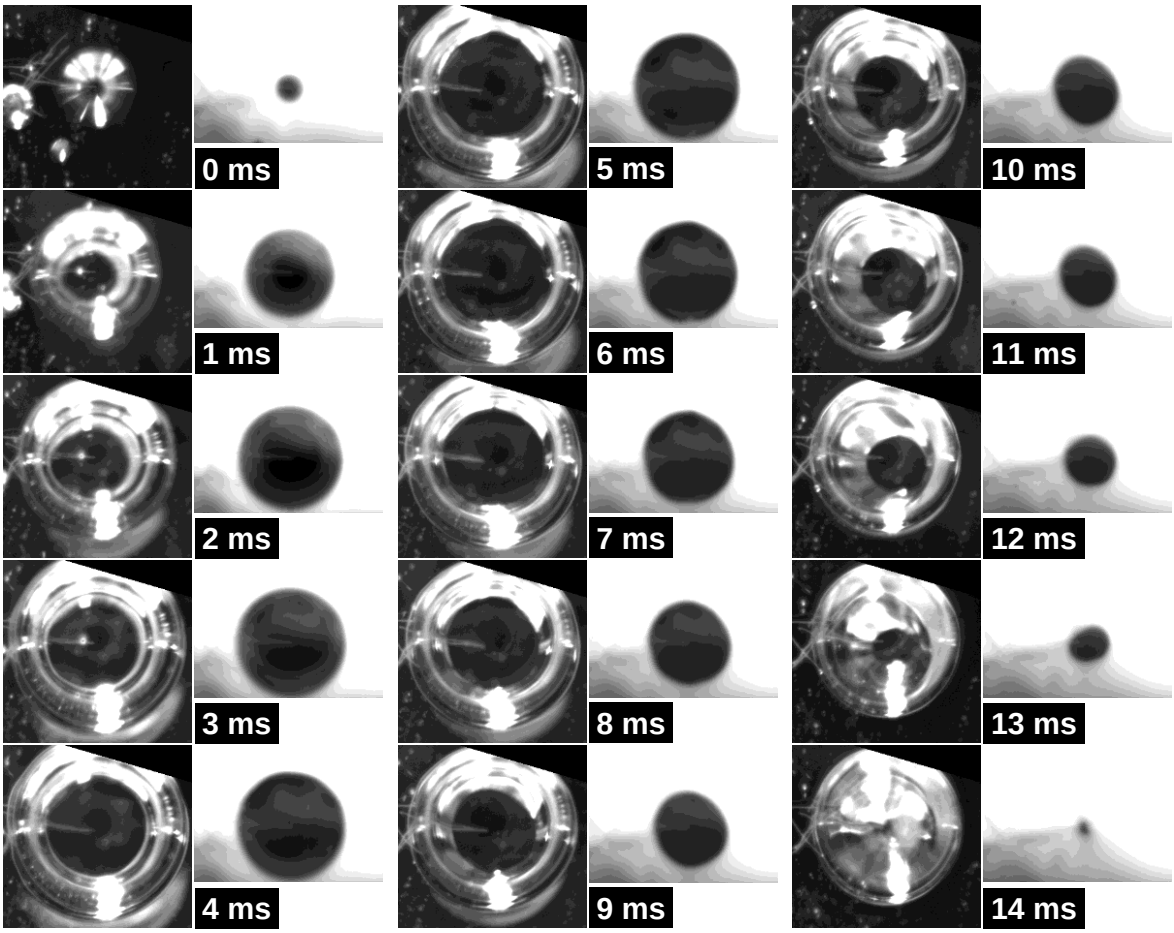

(a)

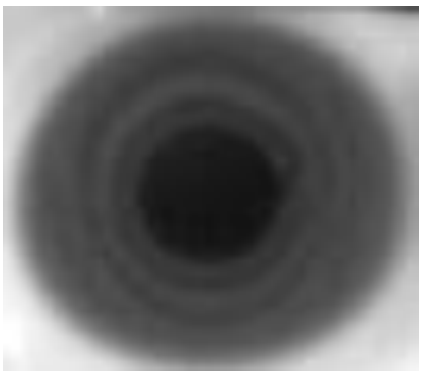

(b)

Figure 11. Bubble nucleation, growth and departure in saturated water on an electrically-heated silicon wafer: (a) synchronized HSV and IR pictures. (b) interference rings are clearly visible between the dry center of the bubble base and the outer wet region of the wafer.

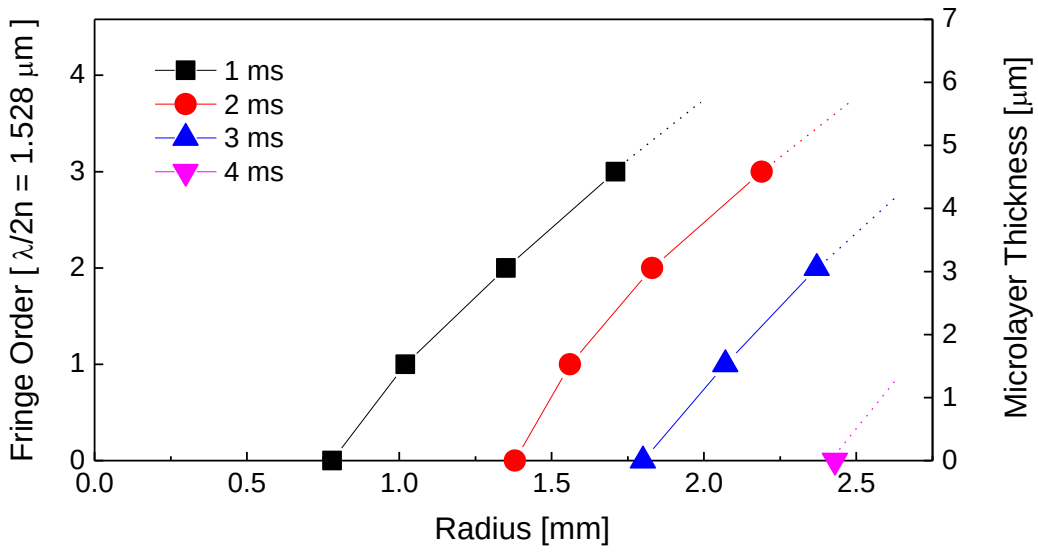

Figure 12. Microlayer shape vs time underneath a growing bubble.